



HAL
open science

Degassing of metamorphic carbon dioxide from the Nepal Himalaya

Matthew J. Evans, Louis A. Derry, Christian France-Lanord

► **To cite this version:**

Matthew J. Evans, Louis A. Derry, Christian France-Lanord. Degassing of metamorphic carbon dioxide from the Nepal Himalaya. *Geochemistry, Geophysics, Geosystems*, 2008, 9, 10.1029/2007GC001796 . insu-03619245

HAL Id: insu-03619245

<https://insu.hal.science/insu-03619245>

Submitted on 25 Mar 2022

HAL is a multi-disciplinary open access archive for the deposit and dissemination of scientific research documents, whether they are published or not. The documents may come from teaching and research institutions in France or abroad, or from public or private research centers.

L'archive ouverte pluridisciplinaire **HAL**, est destinée au dépôt et à la diffusion de documents scientifiques de niveau recherche, publiés ou non, émanant des établissements d'enseignement et de recherche français ou étrangers, des laboratoires publics ou privés.

Copyright

Degassing of metamorphic carbon dioxide from the Nepal Himalaya

Matthew J. Evans

Chemistry Department, Wheaton College, Norton, Massachusetts 02766, USA (evans_matt@wheatonma.edu)

Louis A. Derry

Department of Earth and Atmospheric Sciences, Cornell University, Ithaca, New York 14853, USA

Christian France-Lanord

CRPG-CNRS, Nancy University, Vandoeuvre-les-Nancy, France

[1] Geothermal activity is common at the foot of the Higher Himalaya near the Main Central Thrust (MCT), Nepal Himalaya. We have sampled hot springs along a 150 km stretch of the Himalayan front and find that they carry large fluxes of CO₂ derived from metamorphic reactions. Hot spring fluids are saturated with CO₂, have [DIC] from 1.3 to >100 mmol kg⁻¹ and have δ¹³C_{DIC} values from -13‰ to +13‰(PDB). Analysis of CO₂ released by decrepitation of fluid inclusions from syn- and postdeformational quartz veins indicate that crustal fluids had δ¹³C from -15‰ to +2‰(PDB), consistent with production of CO₂ from both thermal decomposition of organic matter and decarbonation at depth. Modeling of the hot spring fluid compositions indicates that they are strongly degassed. Combining our degassing calculations with estimates of the fraction of hydrothermal alkalinity in local rivers shows that the metamorphic degassing flux of CO₂ in the 32,000 km² Narayani basin of the central Himalaya is >1.3 × 10¹⁰ mol a⁻¹, exceeding the calculated consumption of CO₂ by chemical weathering for the Narayani River basin by a factor of four. Our study implies that the net impact of Himalayan orogenesis on the carbonate-silicate geochemical cycle is not large-scale drawdown of CO₂ because the weathering sink is substantially offset or even exceeded by the metamorphic source.

Components: 10,247 words, 7 figures, 4 tables.

Keywords: metamorphic carbon dioxide; Himalaya; hot springs; carbon cycle.

Index Terms: 1030 Geochemistry: Geochemical cycles (0330); 1041 Geochemistry: Stable isotope geochemistry (0454, 4870); 1034 Geochemistry: Hydrothermal systems (0450, 3017, 3616, 4832, 8135, 8424).

Received 20 August 2007; **Revised** 4 February 2008; **Accepted** 14 February 2008; **Published** 15 April 2008.

Evans, M. J., L. A. Derry, and C. France-Lanord (2008), Degassing of metamorphic carbon dioxide from the Nepal Himalaya, *Geochem. Geophys. Geosyst.*, 9, Q04021, doi:10.1029/2007GC001796.

1. Introduction

[2] The long-term budget of carbon dioxide in the ocean-atmosphere system is controlled by inputs from volcanism, metamorphic devolatilization, and

the oxidation of sedimentary organic carbon. A dynamic balance is maintained by outputs to the sedimentary reservoir, through the processes of chemical weathering of silicate minerals and subsequent precipitation of sedimentary carbonates,

and the burial of organic carbon. An important class of geochemical models has shown that a climate-driven feedback on silicate weathering rates can maintain atmospheric CO₂ within bounds suitable for the presence of liquid water on the Earth's surface [Walker *et al.*, 1981; Berner *et al.*, 1983]. Since the development of early models of the climate-weathering feedback, more recent studies have shown that in at least some settings, silicate rock weathering and CO₂ consumption rates can be a stronger function of physical erosion than of climate [Gaillardet *et al.*, 1999; Riebe *et al.*, 2001; Millot *et al.*, 2002]. These and other studies pose the question whether orogenic events, which occur independently of climate, can drive large increases in CO₂ removal by strongly enhancing erosion rates, and thus act as a strong sink for carbon from the ocean-atmosphere system over time scales of $\geq 10^6$ years. Orogenic events are also believed to drive increases in the flux of CO₂ released to the Earth's surface by metamorphic devolatilization [Barnes *et al.*, 1978; Selverstone and Gutzler, 1993]. Currently, the net impact of orogenic events on the carbonate-silicate portion of the exogenic carbon balance is not well understood but remains a fundamental question in our understanding of the function of the carbon cycle over geologic timescales.

[3] The Himalayan orogen, active across a broad region of south Asia over the last 50 million years, may be considered a "type example" of an orogen produced by continent-continent collision. Erosion fluxes from the Himalaya have been and continue to be large [Curry, 1994; Goodbred and Kuehl, 2000; Clift, 2006]. Silicate weathering of the Himalaya, with its high relief and monsoon climate, has been proposed as a major carbon sink during late Cenozoic time [Raymo and Ruddiman, 1992]. The available data from stream and sedimentary chemistry show that CO₂ consumption across the major Ganges-Brahmaputra basin is elevated over the global average but is ultimately limited by low weathering intensity and the low abundance of Ca and/or Mg silicate minerals [France-Lanord and Derry, 1997; Galy and France-Lanord, 1999; France-Lanord *et al.*, 2003]. Within smaller basins CO₂ consumption may be locally higher [Gardner and Walsh, 1996; West *et al.*, 2002]. While surface processes produce elevated CO₂ consumption rates in the Himalayan orogen, model calculations suggest that the Himalayan collision has resulted in substantial production of CO₂ from metamorphic decarbonation reactions [Selverstone and Gutzler, 1993; Bickle,

1996; Kerrick and Caldeira, 1998; Kerrick, 2001; Gorman and Kerrick, 2006]. However, constraints on the magnitude of this decarbonation flux and its release to the surface are poor. Principally, because of the uncertainties in estimates of degassing fluxes it has not been possible to quantitatively evaluate the relative importance of CO₂ production and CO₂ consumption during Himalayan orogenesis.

[4] Here we provide data from the large Narayani watershed (32,000 km²) of central Nepal that constrain the current rate of degassing of metamorphic carbon dioxide in geothermal systems found along the Main Central Thrust (MCT). We combine fluid inclusion data on metamorphic fluids with data on the chemistry and carbon isotope composition of active hot springs to model the degassing of CO₂ from hydrothermal fluids in the main subbasins of the Narayani. We compare the results of these calculations to independent estimates of the rate of CO₂ consumption in the Narayani by silicate weathering based on stream chemistry [Galy and France-Lanord, 1999; Evans *et al.*, 2004]. Our results show that the rate of CO₂ degassing in geothermal systems of the Narayani is currently larger than the rate of weathering uptake of CO₂ in the same basin.

2. Setting

[5] Along the central Nepal Himalayan front, the high-grade metamorphic rocks of the High Himalayan Crystalline series (HHC) have been thrust over the Paleozoic-Proterozoic marine strata of the Lesser Himalayan sequence (LH) along the Main Central Thrust (MCT) (Figures 1 and 2). Evidence from geomorphology, heat flow, and geologic mapping suggests that deformation and thrust faulting remain active in the region today, although not necessarily along the MCT structure itself [Avouac and Burov, 1996; Lave and Avouac, 2001; Derry and Evans, 2002; Wobus *et al.*, 2003; Hodges *et al.*, 2004; Wobus *et al.*, 2005; Bollinger *et al.*, 2006; Garzanti *et al.*, 2007; Whipp and Ehlers, 2007]. This deformation results in a significant geomorphic break, evidenced in hillslopes and river channels, at the foot of the Higher Himalaya and is characterized by deep gorges carved by the tributaries of the Narayani River as they flow from north to south [Seeber and Gornitz, 1983; Lave and Avouac, 2001; Wobus *et al.*, 2003; Hodges *et al.*, 2004]. Hot springs are ubiquitous along the entire Himalayan front [Barnes *et al.*, 1978] from NW India [Oldham, 1883; Shankar *et al.*, 1991] and Pakistan [Chamberlain *et al.*,

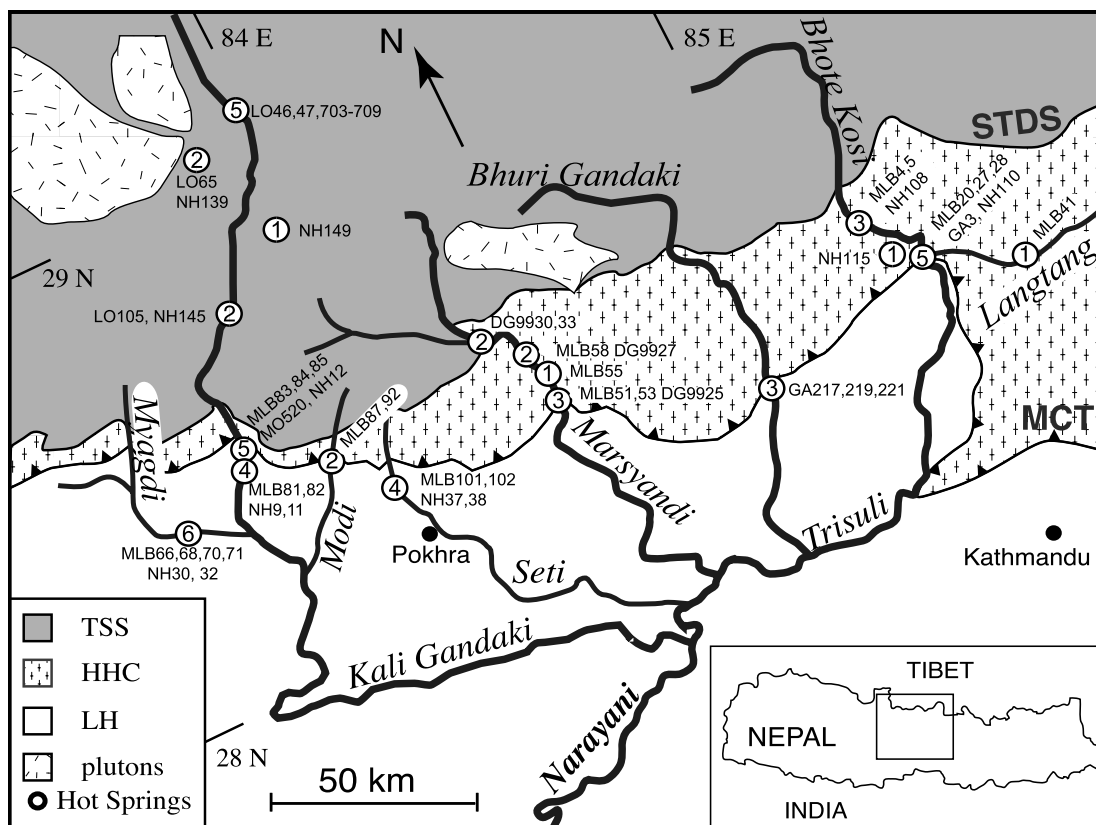


Figure 1. Generalized geologic map (after Colchen *et al.* [1986]) with hot spring locations (open circles). Sampling sites often include several flows from the same spring system. The number within the open circle indicates the number of distinct flows sampled at each location and sample names are labelled at each site. See Table 1 for sample-specific longitude and latitude. Many active hot springs are located near the break in slope at the foot of the Higher Himalaya, often near the trace of the Main Central Thrust. Most springs in this study flow from the High Himalayan Crystalline (HHC) or Lesser Himalayan (LH) formations near the MCT. Springs in the upper Kali Gandaki system flow from the Tethyan Sedimentary Series (TSS) of rocks.

2002] through Nepal (this study) [Bhattarai, 1980; Bogacz and Kotarba, 1981; Kotarba *et al.*, 1981; Colchen *et al.*, 1986; Evans *et al.*, 2004] to Bhutan [Singh *et al.*, 2004] and NE India [Oldham, 1883; Shankar *et al.*, 1991]. In Nepal, the hot springs occur most commonly along stream channels at this break in topography along the Himalayan front. Their position is controlled by the intersection of the deeply incised canyons with the zone of active deformation; the springs are typically distributed over ~10 km of stream reach as the streams cross the MCT zone [Wobus *et al.*, 2003; Evans *et al.*, 2004; Hodges *et al.*, 2004] (Figures 1 and 2). The hot springs are rare or absent in less deeply incised valleys. In our study area exceptions occur in the upper Kali Gandaki where hot springs are present far to the north of the high range and are associated with the graben structure of the Thakola. Our study area spans the entire Narayani River drainage basin and includes

(from east to west) the Myagdi, Kali, Modi, Seti, Marsyandi, Bhuri, and Trisuli (Bhote Kosi) as major streams that incise the Himalayan front and have geothermal activity near the MCT. The Narayani River drainage basin has an area of ca. 32,000 km² (Figure 1).

2.1. Hot Springs

[6] The hot spring fluids have exit temperatures from 30 to 70°C and are at or near calcite saturation, which serves to buffer the pH near neutral. Travertine deposition occurs at the springheads and some sites show massive travertine deposits. Bicarbonate is the dominant form of dissolved CO₂ with concentrations from 1.3 to > 100 mmol kg⁻¹ (Table 1) [Evans *et al.*, 2004]. Waters are supersaturated with CO₂ at the surface and active effervescence is seen at several spring systems (Lo Mantang, Marsyandi, Syabru Bensi, Seti) (Figure 3). The spring fluids are Na⁺-K⁺-HCO₃⁻

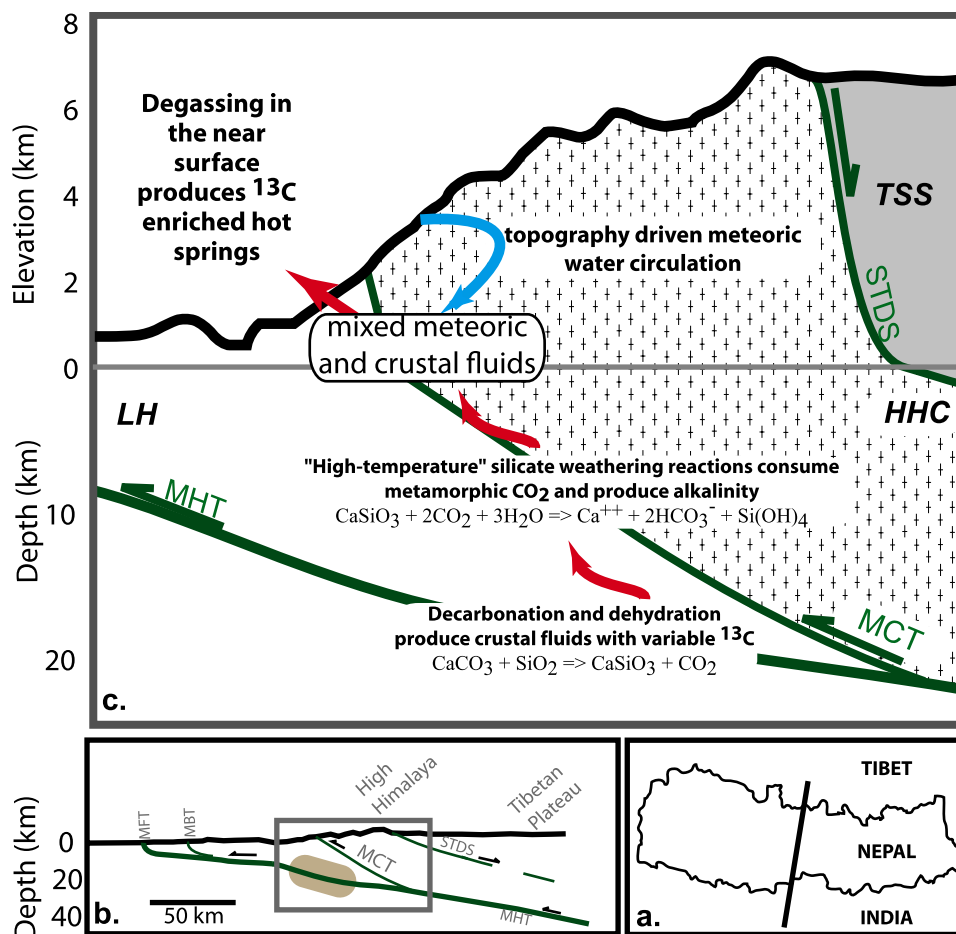


Figure 2. (a) The approximate location of (b) the schematic geological cross section of central Nepal (after *Lave and Avouac* [2001] and *Hodges et al.* [2004]) and (c) topography, idealized fluid flow (in arrows), and example subsurface reactions for the hydrothermal system in central Nepal. Note the change in scale in Figure 2c, with $\sim 4\times$ vertical exaggeration of topography and subsurface structures. Lithologic units are consistent with Figure 1. General location of the area of low resistivity and microseismicity [*Pandey et al.*, 1995; *Lemonnier et al.*, 1999] is shown in brown in Figure 2b. Thrust–sense motion along the Main Central Thrust and related structures has translated warm, high-grade metamorphic rocks of the High Himalayan Crystalline (HHC) series over sedimentary rocks of the Lesser Himalaya (LH). Decarbonation and dehydration reactions in the subducted LH sediments produce CO₂–H₂O fluids at 10–20 km depth, where resistivity data indicate the presence of a fluid phase [*Lemonnier et al.*, 1999]. CO₂-rich fluids migrate up where they are entrained in local meteoric hydrothermal circulation driven by steep geothermal and topographic gradients.

rich, with lesser Ca⁺⁺, Mg⁺⁺, and Cl⁻, and low SO₄⁻ values, and the cationic load is primarily derived from the high temperature alteration of local silicate bedrock at depth [*Evans et al.*, 2004]. Chemical mass balance calculations indicate that the springs currently contribute >10% of the silicate-derived alkalinity flux to the Narayani watershed [*Evans et al.*, 2004]. Only alkalinity derived from silicate weathering is considered here, as alkalinity generated by carbonate weathering has no long-term implications for the ocean-atmosphere carbon balance.

2.2. Quartz Veins

[7] There are at least two generations of quartz veins exposed in outcrop in the MCT zone [*Craw*, 1990; *Pécher*, 1979]. Ductily deformed, syn-metamorphic veins are ubiquitous in the HHC and some units of the LH. These veins lie subparallel to the metamorphic fabric. We take samples of fluid from inclusions in these veins as indicative of the composition of metamorphic fluids mobile during metamorphism and ductile deformation. A later generation of less common quartz veins cross-cuts the metamorphic fabric in both the HHC and

Table 1. Location, Sampling Date, Stable Isotope, and Dissolved Inorganic Carbon Concentrations for Narayani Basin Geothermal Systems [DIC] From Evans et al. [2004]

Sample Name	Location Detail	Sampling Date	Latitude (°N)	Longitude (°E)	Elevation (m)	T (°C)	pH	δD (‰)	δ ¹⁸ O (‰)	δ ¹³ C _{DIC} (‰)	[DIC] (mM)	
	<i>Myagdi Khola</i>											
MLB 68	W. of Beni	4/3/01	28°22.11'	83°30.12'	932	48.6	6.9	-66.5	-8.8	-7.3	21.3	
MLB 66	W. of Beni	4/3/01	28°22.07'	83°30.15'	907	50.7	6.8	-67.7	-9.3	-6.9	12.2	
MLB 70	W. of Beni	4/3/01	28°22.07'	83°30.15'	907	50.7	6.8	-67.8	-9.3	-6.5	13.4	
MLB 71	W. of Beni	4/3/01	28°22.07'	83°30.15'	907	42.4	7.0	-67.7	-9.0	-7.6	14.8	
NH 30	W. of Beni	3/12/95	28°22.07'	83°30.15'	907	52.2	6.5	-67.7	-9.5	-7.2	9.8	
NH 32	W. of Beni	3/13/95	28°22.07'	83°30.15'	907	54.1	6.8				14.0	
	<i>Kali Gandaki</i>											
LO 46	Lo Mantang	5/20/93	29°10.28'	83°58.96	3570			-125.9	-16.7	-1.1	5.6	
LO 47	Lo Mantang	5/20/93	29°10.28'	83°58.96	3550	20.2		-133.7	-16.8	+9.9	36.4	
LO 703	Lo Mantang	7/23/07	29°10.28'	83°58.96	3550	>30		-129.0		+10.3	19.0	
LO 707(Gas) ^a	Lo Mantang	7/23/07	29°10.28'	83°58.96	3550					-2.2 ^a		
LO 65	Tsarang Khola	5/21/93	29°07.77'	83°53.08	3910	12.5		-146.7	-19.7	+11.2	19.9	
NH 139	Tsarang khola	4/30/95	29°07.77'	83°53.08	3865	9.6	6.8	-132.9	-16.9	+9.9	50.1	
NH 149	Narsing	5/2/95	28°54.81'	83°50.90'	2950	14.9	6.5	-113.3	-15.4	+13.5	169.7	
LO 105	Jomosom	5/27/93	28°46.91'	83°43.35	2670	21.2		-113.9	-15.7	-8.4	5.7	
NH 145	Jomosom	5/2/95	28°46.91'	83°43.35	2680	20.4	7.1	-114.0	-15.6	-2.4	87.9	
MLB 85	Tatopani	4/7/01	28°29.78'	83°39.26'		66.4	6.5		-10.5	-0.9	6.4	
MO 520	Tatopani	7/27/98	28°29.78'	83°39.26'						-4.7	5.6	
MLB 83	Ratopani	4/6/01	28°28.68'	83°38.45'	1180	42.8	7.6		-9.5	-13.0	2.2	
MLB 84	Ratopani	4/6/01	28°28.68'	83°38.45'	1180	54.1	7.3		-9.8	-12.8	1.9	
NH 12	Ratopani	3/14/95	28°28.68'	83°38.45'	1120	60	7.4	-69.0	-9.4	-12.7	2.0	
MLB 82	S. of Ratopani	4/6/01	28°27.59'	83°37.65'	1140	37.6	7.9		-9.3	-10.5	1.4	
NH 11	S. of Ratopani	3/14/95	28°27.59'	83°37.65'	1180	49.5	6.7	-69.4	-10.1	-9.4	8.8	
MLB 81	N. of Beni	4/6/01	28°27.47'	83°37.57'	1124	36.1	8.1		-9.5	-9.5	1.5	
NH 9	N. of Beni	3/13/95	28°27.47'	83°37.57'	1124	69.2	6.5	-72.9	-10.0	-1.5	6.4	
	<i>Modi Khola</i>											
MLB 87	Jhinudanda	4/10/01	28°24.94'	83°49.71'		39.3	6.8			+1.9	6.8	
MLB 92	Jhinudanda	4/10/01	28°24.94'	83°49.71'		38.7	7.0		-11.0	+2.0	7.6	
	<i>Seti Khola</i>											
MLB 101	Tatopani	4/13/01	28°21.65'	83°57.61'	1255	45.2	6.5	-78.8		+5.0	54.7	
MLB 102	Tatopani	4/13/01	28°21.65'	83°57.61'	1255	42.5	6.3	-76.8		+5.8	41.5	
NH 37	Tatopani	3/15/95	28°21.65'	83°57.61'	1255	43.1	6.2	-76.0	-10.6	+2.1	16.1	
NH 38	Tatopani	3/15/95	28°21.65'	83°57.61'	1255	41.3	6.5	-75.7	-10.4	+3.7	15.4	
	<i>Marsyandi River</i>											
DG9933	Near Chame	3/1/99	28°31.83'	84°21.05'	2613		7.0	-101.9	-13.9	-3.1	2.6	
DG9930	Near Chame	3/1/99	28°31.83'	84°21.05'	2317		6.0	-101.7	-14.4	+0.8	4.3	
MLB 58	N. of Jagat	3/26/01	28°25.29'	84°24.23'	1283	50.6	7.8		-12.5	-8.2	3.4	

Table 1. (continued)

Sample Name	Location Detail	Sampling Date	Latitude (°N)	Longitude (°E)	Elevation (m)	T (°C)	pH	δD (‰)	$\delta^{18}O$ (‰)	$\delta^{13}C_{DIC}$ (‰)	[DIC] (mM)
DG9927	N. of Jagat	3/1/99	28°25.29'	84°24.23'	1283		6.0	-88.0	-12.7	-11.0	0.9
MLB 55	Ratopani	3/26/01	28°24.78'	84°24.09'	1106	55.2	5.6		-11.7	+11.7	20.1
MLB 51	Bahundanda	3/25/01	28°20.40'	84°23.87'		49.7	6.8		+10.4	+10.8	11.8
MLB 53	Bahundanda	3/25/01	28°20.40'	84°23.87'		47.9	6.2		-10.1	+10.8	36.0
DG9925	Bahundanda	3/1/99	28°20.40'	84°23.87'				-72.0	-10.2	+5.9	47.4
				<i>Bhuri Gandaki</i>							
GA 221	Tatopani	10/23/99	28°16.01'	84°53.42'		52	6.0				7.6
GA 219	S. of Tatopani	10/23/99	28°16.70'	84°53.90'		30	7.0				12.2
GA 217	S. of Tatopani	10/23/99	28°16.70'	84°53.90'		50	6.9	-81.2	-11.4	+3.3	19.1
				<i>Trisuli River</i>							
NH 108	Tatopani on Bhote Kosi	4/13/95	28°14.25'	85°21.50'	1645	62.3	6.6	-87.7	-12.4	+3.2	13.1
MLB 4	Tatopani on Bhote Kosi	3/16/01	28°14.53'	85°21.51'	1714	44.1	6.4		-11.9	+5.6	10.7
MLB 5	Tatopani on Bhote Kosi	3/16/01	28°14.53'	85°21.51'	1714	45.1	6.2	-86.1	-11.9	+6.0	10.3
NH 115	Pargang Gaon	4/14/95	28°12.90'	85°17.78'	2560	48.3	5.6	-81.4	-11.2	+8.3	11.6
MLB 20	Ratopani N. of Syabru Bensi	3/18/01	28°11.01'	85°20.62'		24.4	5.7		-11.0	+13.2	7.1
GA 3	Syabru Bensi	10/4/99	28°9.74'	85°20.21'	1425	54	6.7		-10.9	+5.5	17.1
MLB 27	Syabru Bensi	3/19/01	28°9.74'	85°20.21'	1425	53.9	6.6	-80.9	-11.1	+6.4	19.1
MLB 28	Syabru Bensi	3/19/01	28°9.74'	85°20.21'	1425	68.7	6.6	-83.2	-11.4	+6.2	20.6
NH 110	Syabru Bensi	4/14/95	28°9.74'	85°20.21'	1425	68.5	6.7	-82.2	-11.6	+5.7	19.2
MLB 41	Langtang Khola	03/20/01	28°9.10'	85°22.38'		41.2	8.6		-13.8	-4.8	5.0
				<i>Outside of Narayani Basin</i>							
NH 120	Khar Khola	4/18/95	28°01.07'	84°32.79'	520	34.8	10.1	-51.4	-7.8	-14.1	75.8
NH 21	Bhote Kosi at Kodari	3/16/95	27°57.00'	85°57.00'		46.4	6.4	-78.1	-10.4	-8.7	8.3

^aSample LO 707, $\delta^{13}C$ is reported for $CO_2(g)$.



Figure 3. Photo of effervescing CO₂-rich spring along the Marsyandi River (sample MLB-51). $T_{\text{fluid}} = 55^{\circ}\text{C}$, $\delta^{13}\text{C}_{\text{DIC}} = +11.6\text{‰}$, $P_{\text{CO}_2} > 1$ bar. The spring is surrounded by extensive travertine (CaCO₃) deposits.

LH and has euhedral quartz crystals and open fracture filling textures. These veins formed at temperatures below the brittle-ductile transition, or below about 350°C.

3. Methods

[8] Most hot spring samples were taken over 6 weeks in the spring of 2001; however, a number of sites had been sampled and analyzed previously, providing repeat sampling of several key springs (Table 1). Waters collected for stable isotope and anion analysis were filtered on-site with 0.22 μm mixed ester filters and stored in acid-washed polyethylene bottles. To assure sample integrity, samples were taken with no headspace and were temporarily stored at temperatures below the sampling temperature until they could be refrigerated at <4°C. Temperature and pH were measured at the time of sampling using a combined pH and temperature probe on a portable field meter (Beckman Coulter Phi 295). Data and procedures used to estimate stream and hot spring alkalinity fluxes are described in detail in the work of *Evans et al.* [2004]. One gas sample was taken at the Lo Mantang site using a funnel and tubing setup to

drive the gas into a copper tube, which was then sealed by metal clamps.

[9] The $\delta^{13}\text{C}$ of dissolved inorganic carbon was measured on CO₂ released by acidification of an aliquot of the water samples with phosphoric acid [*Galy and France-Lanord, 1999*]. The δD and $\delta^{18}\text{O}$ of water were respectively measured by a continuous flow technique using a Cr reduction reactor and CO₂-water equilibration [*Gajurel et al., 2006*]. CO₂ and H₂O were extracted from fluid inclusions by crushing under vacuum 1 to 5 g of clean quartz-vein material in a stainless steel tube. CO₂ and H₂O were then separated by cryogenic methods. The δD of fluid inclusions was measured after reduction of decrepitated water over hot uranium and $\delta^{18}\text{O}$ of quartz veins was analyzed by BrF₅ fluorination. The isotopic values were determined using VG 602D and GV Isoprime mass spectrometers at the Centre de Recherches de Pétrographiques and Géochimiques (CRPG) in Nancy, France. Reproducibility based on multiple analyses of a single sample are as follows: for $\delta^{13}\text{C}$ values: $\pm 0.3\text{‰}$, for $\delta^{18}\text{O}$ values: $\pm 0.2\text{‰}$, and for δD values: $\pm 2\text{‰}$. Results are reported relative to PDB (Peedee belemnite) for carbon and V-SMOW for oxygen and hydrogen.

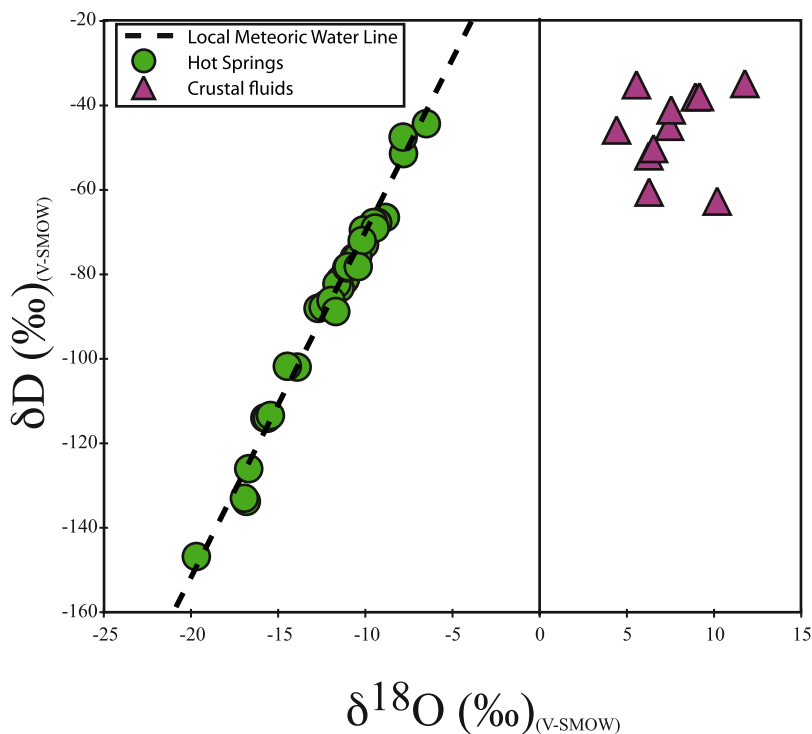


Figure 4. The δD and $\delta^{18}\text{O}$ of hot spring fluids and fluid inclusion fluids from this study and the local meteoric water line for central Nepal [Garzione *et al.*, 2000; Gajurel *et al.*, 2006]. The hot springs do not vary significantly from the meteoric water line defined by local surface waters and precipitation ($\delta\text{D} = 8.16 \times \delta^{18}\text{O} + 10.7$), indicating a large water/rock ratio. The fluid inclusions plot well to the right of the local meteoric water line, consistent with a metamorphic source.

[10] The gas sample was analysed for both molecular composition and $\delta^{13}\text{C}$ of CO_2 . The sample was passed through a trap at -70°C to remove water vapor. A fraction of the sample was analyzed on a gas source mass spectrometer using electromagnet scanning from mass 2 to 70 to identify species present in the sample. Carbon dioxide was separated from “noncondensable” gases using a cryogenic trap at -180° . The CO_2 fraction was quantified by manometry and analyzed for $\delta^{13}\text{C}$ as above.

4. Results

4.1. Fluids

[11] Oxygen and hydrogen isotopic analyses of the hot spring fluids (Table 1) fall closely along the local meteoric water line (Figure 4), in agreement with previous work [Grabczak and Kotarba, 1985]. Crustal fluids at depth were sampled by fluid inclusions, and have a nonmeteoric source (Figure 4). For the fluid inclusions the δD of the fluid released by decrepitation is measured directly. To calculate the $\delta^{18}\text{O}$ of the trapped fluid from analyses of the $\delta^{18}\text{O}$ of quartz we assume that the

fluid was in isotopic equilibrium with the host quartz and use equilibrium fractionation factors from Clayton *et al.* [1972]. For the postmetamorphic fracture-filling veins we use homogenization temperatures from the fluid inclusions to constrain the temperature of equilibration, and these are close to 300°C [Darling *et al.*, 2003]. For the syn-deformational veins the homogenization temperatures are not available. We estimate equilibration temperatures of $350\text{--}400^\circ\text{C}$ based on the ductile behaviour of quartz and the mineral assemblages of the host rocks [France-Lanord, 1987]. The uncertainty in the equilibration temperature for these samples produces an uncertainty in the estimated $\delta^{18}\text{O}$ of the trapped fluid of about 1.2‰ and has little impact on our conclusions. The fluids trapped by both generations of inclusions are well to the right of the MWL (Figure 4) and indicate both the ductile and brittle phase quartz veins contain a metamorphic fluid phase. The metamorphic fluid phase sampled by the inclusions is CO_2 -rich, with X_{CO_2} from 0.07 to 0.37 [Darling *et al.*, 2003], in agreement with previous studies by Pêcher [1979] and Craw [1990].

Table 2. Basic Lithologic Character and Carbon Isotope Values for Carbonates and Pelites From the Lesser Himalaya

	Latitude (°N)	Longitude (°E)	% Organic Carbon		$\delta^{13}\text{C}$ Organic Carbon	
			Calcite	Dolomite	Calcite	Dolomite
<i>LH Carbonates</i>						
AP 168	28°0.05'	84°0.53'	79.0		-0.1	
AP 207	28°0.16'	84°0.7'	12.7	47	-1.9	-1.7
AP 811	28°0.21'	85°0.13'	31.5	31	-3.5	-2.7
AP 816	28°0.23'	85°0.13'	16.8	19	-1.2	-0.3
AP 865	27°0.98'	84°0.27'	12.5	58	-1.4	-1.3
AP 867	28°0.01'	84°0.26'	17.0	65	-1.1	-0.9
<i>LH Pelites</i>						
AP 28	28°0.13'	83°0.91'		7.51		-28.9
AP 874	28°0.06'	84°0.25'		0.19		-26.1
AP 969	28°0.06'	84°0.35'		0.15		-21.9
AP 972	28°0.03'	84°0.35'		0.14		-26.7
NL 1	27°0.82'	84°0.79'		10.34		-31.0
<i>Biotite Zone</i>						
AP 167	28°0.05'	84°0.53'		0.08		-21.6
AP 385	27°1.00'	84°0.89'		0.06		-22.3
AP 390	27°0.97'	84°0.97'		0.1		-22.0
AP 417	27°0.94'	84°0.85'		0.44		-28.6
AP 537	27°0.92'	84°0.63'		0.06		-23.7
AP 888	28°0.19'	84°0.29'				-21.9
NL 3	27°0.88'	84°0.75'		0.01		-25.4
NL 4	27°0.93'	84°0.74'		0.03		-23.6
<i>Garnet Zone</i>						
AP 199	28°0.09'	84°0.66'		0.06		-21.5
AP 375	28°0.06'	84°0.77'		0.07		-23.1
AP 440	28°0.05'	84°0.9'		0.05		-21.5
AP 657	28°0.11'	84°0.55'		0.02		-24.3
<i>Staurolite Zone</i>						
AP 346	28°0.13'	84°0.75'		0.11		-18.7
AP 473	28°0.20'	84°0.91'		0.06		-19.9
AP 825	28°0.21'	85°0.12'		6.36		-28.6

[12] Geophysical methods have been used to infer the presence of a fluid phase along the MCT-MHT structure directly under our study area (Figure 2). *Lemonnier et al.* [1999] used magnetotelluric (MT) data to identify a zone of high conductivity at approximately 20 km depth that they inferred to indicate the presence of a crustal fluid derived from prograde metamorphic reactions. The MT survey was conducted through a part of our study area, and MT sounding stations were located near the zone of geothermal activity we sampled along the Trisuli River at the village of Syrabu Bensi. Thus there is direct evidence for the presence of a deep crustal fluid beneath the geothermally active zone associated with the surface trace of the MCT in our study area. The fluid-rich zone coincides with the position of a zone of focused microseismicity at an

inferred crustal ramp along the MHT [*Schelling and Arita*, 1991; *Pandey et al.*, 1995; *Lave and Avouac*, 2001].

[13] The major element chemistry of the hot springs also suggests that metamorphic volatiles may be entrained in the meteoric water circulation that feeds the hot spring fluids. *Evans et al.* [2004] noted that some hot springs sampled in this study have excess chloride (significantly above what can be accounted for from atmospheric deposition or halite dissolution) and proposed that the excess Cl^- is derived from a HCl phase in a metamorphic crustal fluid. Neutralization of H^+ by water-rock interaction would leave a Cl^- enriched fluid such as observed in springs along the Marsyandi River. Helium isotope data further support a crustal origin for the volatiles in the Nepal hot springs. *Marty et*

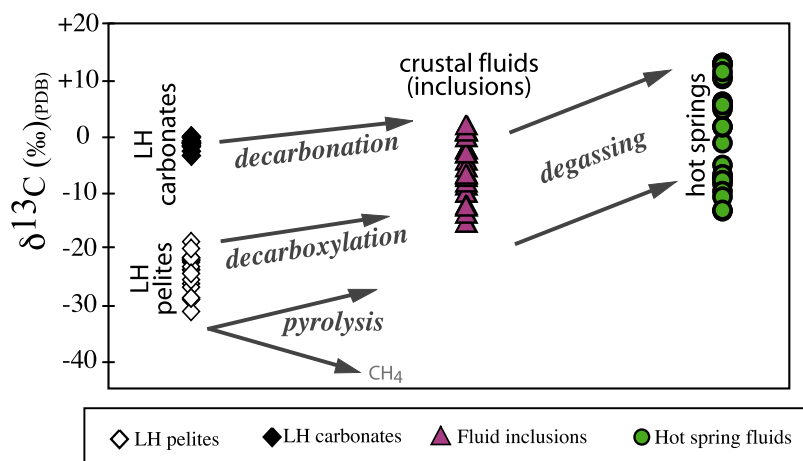


Figure 5. Schematic generation and evolution of $\delta^{13}\text{C}$ in Himalayan source rocks and crustal fluids with measured $\delta^{13}\text{C}$ values for rocks, crustal fluids, and hot springs. LH carbonate and pelite data are whole rock measurements of carbonate and organic carbon, respectively. Crustal fluids as sampled by fluid inclusion data are from decrepitation release of CO_2 from both ductily and brittly deformed quartz veins in LH host rocks. Prograde metamorphism of carbonates produces ^{13}C -enriched fluids, while thermal decarboxylation and pyrolysis of organic matter produces both ^{13}C enriched CO_2 and ^{13}C depleted methane, with CO_2/CH_4 depending on local redox control. The result is crustal fluids with a range of $\delta^{13}\text{C}$ as observed in fluid inclusion data. The spread in hot spring $\delta^{13}\text{C}_{\text{DIC}}$ reflects this range, modified by variable degrees of near-surface degassing that drives $\delta^{13}\text{C}_{\text{DIC}}$ in the residual fluids to high values.

al. [1996] report helium isotope ratios from some of the springs we sampled, and found very low $^3\text{He}/^4\text{He}$ (0.0014–0.14 R_a , where R_a is the atmospheric ratio). These data clearly indicate a crustal source for the volatiles, with little or no mantle input.

[14] The gas phase sampled at Lo Mantang (LO 707) contained 8 molar % of N_2 and O_2 with N_2/O_2 ratio similar to air and traces of Ar. The remaining phase, released between -180° and -70°C , is pure CO_2 . Other gases such as CH_4 , H_2S or SO_2 were not detected in the sample.

4.2. Carbon Isotopic Compositions

[15] Carbon isotope measurements of the dissolved inorganic carbon (DIC) in the hot spring waters show a wide range of $\delta^{13}\text{C}_{\text{DIC}}$ from -13‰ to $+13\text{‰}$, (Table 1, Figure 5). DIC concentrations range from 1 to 170 mmol/kg and there is no simple relationship between $\delta^{13}\text{C}_{\text{DIC}}$ and [DIC]. Spring fluids in the Lo Mantang, Seti, Modi, Marsyandi, Bhuri, and Trisuli systems have positive $\delta^{13}\text{C}_{\text{DIC}}$ from +2 to $+13\text{‰}$, while the Myagdi and Lower Kali springs have high DIC (2–20 mM) but negative $\delta^{13}\text{C}_{\text{DIC}}$ (Table 1). Repeat sampling of a number of spring sites over a several year period suggests that while both spring chemistry and isotopic composition show some variability, the values are broadly stable from year to year (Table 1). The enriched $\delta^{13}\text{C}_{\text{DIC}}$ values are among the highest

values ever reported for geothermal waters, similar to values for waters and associated travertines in Yellowstone [Friedman, 1970], Utah [Shipton *et al.*, 2004], Poland [Dulinski *et al.*, 1995], and Italy [Pentecost, 1995; Guo *et al.*, 1996].

[16] There are no known sources of CO_2 in our study area for the hot spring fluids that have sufficiently high $\delta^{13}\text{C}$ to account for the observed enriched $\delta^{13}\text{C}_{\text{DIC}}$ values in the hot springs. The LH in Central Nepal contains a carbonate unit, but $\delta^{13}\text{C}$ from this unit range from -3.5 to -0.1‰ ($\bar{X} = -2\text{‰}$), and central Nepal pelites containing graphitic or organic carbon have $\delta^{13}\text{C}$ from -31 to -19‰ (Table 2, Figure 5). We therefore infer that the source of the high CO_2 in the sampled fluids is the entrainment of a small amount of metamorphic fluid, as constrained by the fluid inclusion data, into the meteoric circulation system. Mixing of only around 1% of a CO_2 -rich metamorphic fluid into the meteoric circulation can readily produce a fluid with high CO_2 concentrations but with meteoric δD and $\delta^{18}\text{O}$ values. As noted above, the observation of a large fluid reservoir directly beneath the geothermally active zone, evidence for the inclusion of crustal volatiles in the hot spring fluids, and the presence of metamorphic fluids at relatively shallow levels in the crust (<3 km, [Darling *et al.*, 2003]) all are consistent with the incorporation of CO_2 from a deep crustal source into the meteoric circulation

Table 3. Stable Isotope Values for Fluid Inclusions Where δD and $\delta^{13}C$ Reflect Isotopic Composition of the Fluid Inclusion Fluids While $\delta^{18}O$ Quartz Is That of the Vein Quartz^a

Sample Name	Latitude (°N)	Longitude (°E)	δD (‰)	$\delta^{18}O$ Quartz (‰)	$\delta^{13}C$ (‰)
GA 10	28°09.99'	85°19.57'	-58.9		-2.0
MLB 33	28°9.76'	85°19.92'	-50.9		-2.7
MLB 74	28°21.72'	83°30.81'	-57.9		
MLB 77	28°24.64'	83°35.90'	-32.2		
MLB 80	28°26.02'	83°36.07'	-50.4	13.8	
MLB 90	28°24.94'	83°49.71'	-62.4		0.1
GA 204	28°19.78'	84°54.11'	-46.2	11.7	-7.9
GA 210	28°18.73'	84°54.21'	-49.7		-6.9
MLB 89	28°24.94'	83°49.71'	-63.4		1.1
MLB 9	28°14.76'	85°21.77'	-42.0		-11.9
MLB 34	28°9.75'	85°19.85'	-60.5	13.6	-6.5
GA 75	28°22.00'	85°19.00'	-62.7	17.6	2.3
GA 69	28°22.00'	85°19.00'	-55.7		-12.1
AP 208	28°0.16'	84°0.7.00'		14.9	1.2
AP 231	28°0.22'	84°0.74'		12.2	-6.3
AP 416	27°0.94'	84°0.84'		13.3	
AP 491				11.6	
AP 725	28°0.25'	84°0.91'		11.6	
AP 747	28°0.22'	84°0.99'		11.3	
AP 810	28°0.22'	85°0.13'		11.5	-15.0
U 107	28°0.27'	84°0.9'		11.4	-8.4
NL 10	28°0.17'	84°0.88'	-55		
NL 15	28°0.17'	84°0.88'	-52	10.7	-4.0
NL 17	28°0.20'	84°0.88'	-35	10.0	-5.2
NL 26	28°0.27'	84°0.90'	-41	12.0	-9.7
NL 400	28°0.32'	83°0.94'	-38	13.4	
NL 401	28°0.33'	83°0.94'		15.6	
NL 508	28°0.37'	83°0.99'		11.9	
NL 542			-92	21.9	1.9
NL 601	28°0.26'	84°0.2'	-45	11.9	-13.4
NL 603	28°0.26'	84°0.22'	-35	16.2	-2.7
NL 605	28°0.29'	84°0.38'		18.4	-2.0
NL 633	28°0.30'	84°0.40'	-38	13.6	1.3

^a Sample NL 542 from *Boullier et al.* [1991], remaining samples labeled NL, AP, or U from unpublished dissertations of *France-Lanord* [1987] (NL, AP, or U) and *Evans* [2002] (MLB and GA).

system that produces the geothermal flow. The presence of these mixed metamorphic and meteoric fluids is well documented in other active collisional orogens, as meteoric water is driven down by topographic gradients and metamorphic fluids move upwards along steep thermal gradients [*Koons and Craw*, 1991; *Jenkin et al.*, 1994; *Templeton et al.*, 1998; *Whipp et al.*, 2007].

4.2.1. The $\delta^{13}C$ Variability and Processes of Carbon Isotopic Enrichment

4.2.1.1. Metamorphism

[17] CO_2-H_2O fluids with a wide range of $\delta^{13}C_{CO_2}$ values can be produced by decarbonation, pyrolysis, and dehydration of the mixed pelite-carbonate lithologies of the Lesser Himalaya during prograde metamorphism (Figure 5). CO_2 -rich fluids produced during metamorphic decarbonation are enriched in ^{13}C over the source rock, with a maximum

fractionation estimated at +3.8‰ at about 500°C [*Chacko et al.*, 1991]. Assuming that the substrate carbonate minerals have a typical LH value = -2‰, decarbonation reactions could produce a CO_2 fluid with $\delta^{13}C$ near +2‰. Thermal decomposition (pyrolysis) of kerogen produces mixed CO_2-CH_4 fluids, with the ratio of CO_2/CH_4 strongly dependent on the Fe^{3+}/Fe^{2+} of the host rock [*Giggenbach*, 1997]. The isotopic composition of CO_2 from such fluids can be quite variable, depending on the CO_2/CH_4 ratio and the relative importance of equilibrium versus kinetic isotope effects. In the absence of open system fractionation such fluids will not produce highly ^{13}C -enriched CO_2 . Mixing of fluids with CO_2 derived from both decarbonation and pyrolysis sources can produce a broad range of $\delta^{13}C_{CO_2}$.

[18] The $\delta D-\delta^{18}O$ data from fluid inclusions sampled for this study indicate that they trapped metamorphic fluid. The $\delta^{13}C$ of the CO_2 in vein

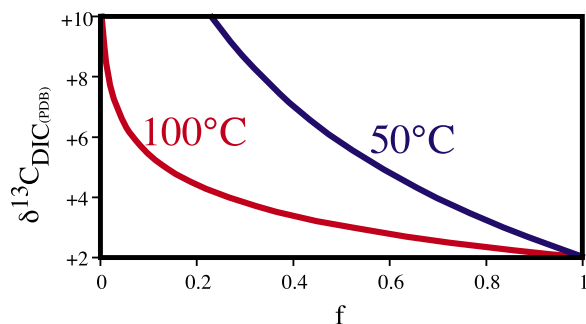


Figure 6. Schematic model results for degassing CO_2 from a hot spring fluid with an initial $\delta^{13}\text{C}_{\text{DIC}} = +2\text{‰}$ using Rayleigh fractionation for $\text{HCO}_3^-(\text{aq}) - \text{CO}_2(\text{g})$ at $T_{\text{fluid}} = 50^\circ$ and 100°C (equation (1)). The initial $\delta^{13}\text{C}_{\text{DIC}} = +2\text{‰}$ is consistent with a decarbonation fractionation of 3.8‰ from LH carbonate values (-2‰), as well as the maximum observed fluid inclusion values (Tables 1–4). Degassing produces ^{13}C -depleted $\text{CO}_2(\text{g})$, leaving the residual DIC with relatively high $\delta^{13}\text{C}_{\text{DIC}}$. To produce $\delta^{13}\text{C}_{\text{DIC}}$ of $+6$ to $+12\text{‰}$ (similar to the observed values at some springs) requires loss of 50 – 99% dissolved CO_2 by degassing ($f = 0.5$ to 0.01), depending on the temperature at which $\text{CO}_2(\text{g})$ is separated.

fluid inclusions should therefore be a good indication of the composition of carbon in crustal fluids produced during prograde metamorphism and should reflect the expected variability from both decarbonation and pyrolysis reactions. Crushing experiments on fluid inclusions from syn- and postdeformational quartz veins in the LH and HHC rocks confirm this expectation, with $\delta^{13}\text{C}_{\text{CO}_2}$ in the inclusions ranging from -15.0 to $+2.3\text{‰}$ (Table 3). The maximum $\delta^{13}\text{C}$ value observed in the fluid inclusions ($+2.3\text{‰}$) is consistent with decarbonation-derived CO_2 from an initial carbonate substrate with $\delta^{13}\text{C}$ near -2‰ , identical to LH carbonates. There is no fluid inclusion evidence for extremely enriched $\delta^{13}\text{C}_{\text{CO}_2}$ values such as those observed in some of the hot springs.

4.2.1.2. Degassing

[19] While metamorphic decarbonation can produce a modestly ^{13}C enriched fluid, this mechanism cannot produce the very high $\delta^{13}\text{C}_{\text{DIC}}$ observed in many Himalayan springs. An additional mechanism is necessary. Open-system degassing of CO_2 from an aqueous fluid in the near-surface environment can substantially alter the $\delta^{13}\text{C}_{\text{DIC}}$ of the remaining fluid [Friedman, 1970; Dandurand et al., 1982; Michaelis et al., 1985; Amundson and Kelly, 1987; Chafetz et al., 1991; Dulinski et al., 1995; Guo et al., 1996]. As supersaturated fluids

approach the surface they can degas; in some cases P_{CO_2} in the fluid exceeds $P_{\text{hydrostatic}}$, producing effervescence (Figure 3). At the circum-neutral pH's of the springs, HCO_3^- is the dominant form of dissolved CO_2 and the carbon isotope fractionation factor between dissolved bicarbonate and $\text{CO}_2(\text{g})$ is positive below $\sim 125^\circ\text{C}$ [Mook et al., 1974]. Open system degassing at temperatures below 125°C will steadily increase the $\delta^{13}\text{C}_{\text{DIC}}$ value of the residual fluid as ^{13}C -depleted $\text{CO}_2(\text{g})$ is evolved and separated. If open-system degassing is responsible for the high $\delta^{13}\text{C}_{\text{DIC}}$ values observed in the springs, the degassing must occur between 125°C and the observed temperature of the springs at the surface (30 – 70°C).

[20] Carbon isotope fractionation resulting from open system degassing can be modeled as a Rayleigh process:

$$R_{\text{DIC}} = R_{\text{DIC}}^0 f^{(\frac{1}{\alpha}-1)} \quad (1)$$

where R_{DIC}^0 is the carbon isotope ratio of the DIC in the initial fluid, R_{DIC} is the carbon isotope ratio of DIC after degassing, $\alpha =$ the temperature dependent fractionation between $\text{HCO}_3^-(\text{aq})$ and $\text{CO}_2(\text{g})$, and $f =$ the fraction of CO_2 remaining after degassing. Degassing modeled at 100°C and 50°C illustrates the amount of CO_2 loss required to produce the high-observed $\delta^{13}\text{C}_{\text{DIC}}$ of the fluids (Figure 6). Fractionation between $\text{HCO}_3^-(\text{aq})$ and $\text{CO}_2(\text{g})$ is $+1.5\text{‰}$ at 100°C and $+5.5\text{‰}$ at 50°C [Mook et al., 1974]. Taking a simple case of a LH carbonate with $\delta^{13}\text{C} \approx -2\text{‰}$ (Table 2), decarbonation should produce a fluid with a maximum $\delta^{13}\text{C}$ of $+2\text{‰}$ (Table 3). Using this as our initial fluid in equation (1), degassing at 50°C will produce DIC at $+10\text{‰}$ after 77% CO_2 loss ($f = 0.23$) (Figure 6). At 100°C , the same initial fluid must be essentially completely degassed (99.5% CO_2 loss, $f = 0.005$) in order for the solution to reach $+10\text{‰}$ (Figure 6).

[21] The spring fluids are supersaturated with respect to calcite, and travertine deposition occurs at the discharge sites. A more realistic description of the isotopic fractionation includes the effects of calcite precipitation associated with degassing. At the observed spring pHs bicarbonate ion is the main component of DIC, so we can write



[22] The isotopic fractionation resulting from the combined loss of DIC as calcite and $\text{CO}_2(\text{g})$ can be expressed as the combination of the fractionation

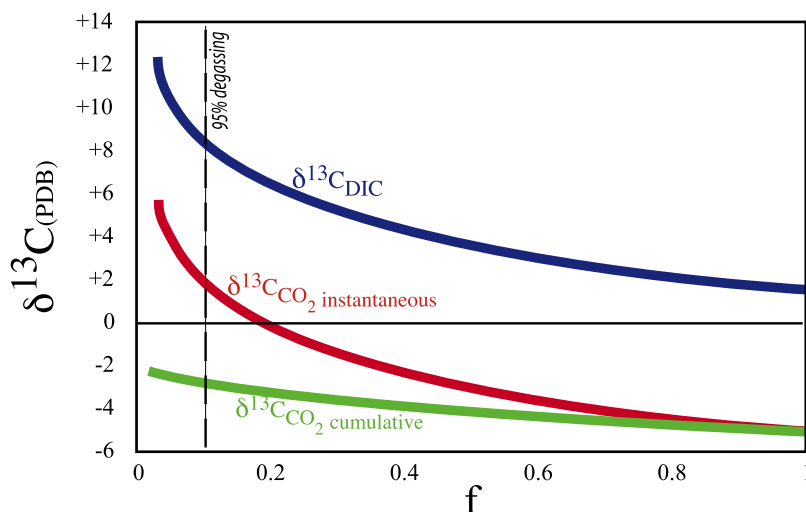


Figure 7. Degassing model for Lo Mantang hot springs using equations (2)–(6). Measured values for $\delta^{13}\text{C}_{\text{DIC}} = +10.3\text{‰}$, $\delta^{13}\text{C}_{\text{CaCO}_3} = +8.8$ to $+10.8\text{‰}$, $\delta^{13}\text{C}_{\text{CO}_2} = -2.2\text{‰}$. Blue curve shows calculated evolution for $\delta^{13}\text{C}_{\text{DIC}}$. Red curve shows calculated instantaneous values for $\delta^{13}\text{C}_{\text{CO}_2}$. Green curve shows calculated cumulative $\delta^{13}\text{C}_{\text{CO}_2}$. The calculation assumes an initial fluid with $\delta^{13}\text{C}_{\text{DIC}} = +1.5\text{‰}$, with fractionation factors for $\text{HCO}_3^- - \text{CO}_2$ and $\text{CaCO}_3 - \text{CO}_2$ calculated for 40°C . Approximately 95% C loss as calcite and $\text{CO}_2(\text{g})$ (marked with the dashed line) is required to produce the observed values in the fluid, solid, and gas phases.

factors for bicarbonate – $\text{CO}_2(\text{g})$ and calcite – $\text{CO}_2(\text{g})$.

$$\frac{-\alpha_{\text{HCO}_3^- - \text{CO}_2} + (\alpha_{\text{CaCO}_3 - \text{CO}_2} - \alpha_{\text{HCO}_3^- - \text{CO}_2})}{2} = \alpha_{\text{C}_{\text{loss}} - \text{HCO}_3^-} \quad (3)$$

The isotopic composition of bicarbonate remaining in solution after calcite precipitation and degassing is then

$$\delta_{\text{HCO}_3^-} = 1000f(\alpha_{\text{C}_{\text{loss}} - \text{HCO}_3^-} - 1) + \delta_i \quad (4)$$

where f is the fraction of HCO_3^- remaining in solution and δ_i is the initial isotopic composition of the fluid.

[23] The isotopic composition of the instantaneous fraction of CO_2 degassed is

$$\delta_{\text{CO}_2}^{\text{instant}} = \delta_{\text{HCO}_3^-} \times 1000 \ln \alpha_{\text{HCO}_3^- - \text{CO}_2} \quad (5)$$

The cumulative isotopic composition of the $\text{CO}_2(\text{g})$ phase (assuming no back-reaction) is

$$\delta_{\text{CO}_2}^{\text{cum}} = \frac{\delta_i - f \times \delta_{\text{HCO}_3^-} - (1-f)/2 \times 1000 \ln \alpha_{\text{CaCO}_3 - \text{CO}_2}}{1-f} \quad (6)$$

$\text{CO}_2(\text{g})$ formed by reaction (2) with the instantaneous isotopic composition given by (5) in the

subsurface may not evade immediately but rather mix with other increments of gas before evasion at the surface. Such a phase should have an isotopic composition approaching that defined by equation (6).

[24] At the Lo Mantang site DIC, $\text{CO}_2(\text{g})$ and travertine were collected and analyzed for $\delta^{13}\text{C}$, providing a relatively complete picture of the degassing process. Here $\delta^{13}\text{C}$ is high in both DIC ($+10.3\text{‰}$) and travertine ($+8.8$ to $+10.8\text{‰}$). Coexisting $\text{CO}_2(\text{g})$ has a $\delta^{13}\text{C} = -2.2\text{‰}$ (Table 1), indicating strong fractionation between the fluid and vapor phases. Application of equations (3)–(6) using fractionation factors at 40°C [Mook *et al.*, 1974; Romanek *et al.*, 1992; Szaran, 1997] constrains the degassing process (Figure 7). For the Lo Mantang springs, these equations and the observations can only be satisfied simultaneously if $\delta_i \leq 1.5\text{‰}$, resulting in $f = 0.05$ (95% C loss). Higher temperatures and/or lower δ_i would require greater CO_2 loss. In general we would expect measured $\delta^{13}\text{C}_{\text{CO}_2}$ values to lie between the instantaneous value and the cumulative value. The measured $\delta^{13}\text{C}$ of the Lo Mantang gas sample is close to the expected value for the cumulative $\text{CO}_2(\text{g})$ fraction, suggesting that the $\text{CO}_2(\text{g})$ produced is not immediately degassed, consistent with the observation of gas supersaturation at Lo Mantang (and other springs).

Table 4. Calculated CO₂ Fluxes From the Central Nepal Spring Systems^a

	[DIC] (mmol/kg)	δ ¹³ C _{DIC} (‰)	Q _{HS} ^b (×10 ⁶ m ³ a ⁻¹)	Average Exit T (°C)	Direct DIC Flux (×10 ⁹ mol a ⁻¹)	F _{exit T}	ΣCO ₂ flux (×10 ⁹ mol a ⁻¹)
Myagdi Khola	15.4	-7.1	11.2	48	0.21		0.21
Kali Gandaki	3.0	-9.0	39.6	50	0.13		0.13
Modi Khola	8.2	+1.9	10.3	39	0.10		0.10
Seti Khola	48.2	+5.4	1.6	44	0.12	0.69	0.40
Marsyandi	12.0	+11.0	9.1	52	0.34	0.97	10.6
Bhuri Gandaki	19.2	+3.3	1.2	50	0.03	0.39	0.05
Trisuli	15.2	+6.0	21	53	0.50	0.79	2.38
SUM					1.4		13.9

^aFor the Myagdi Khola, Kali Gandaki, and Modi Khola (δ¹³C_{DIC} < +2‰), CO₂ flux is assumed to be DIC only. The CO₂ flux from springs with δ¹³C_{DIC} > +2‰ reflects the combined degassing and DIC contributions, with degassing and associated calcite precipitation assumed to take place entirely at the observed exit temperature. F_{exit T} is the required fraction CO₂ loss (by degassing and calcite precipitation at the exit T) to produce the measured δ¹³C_{DIC}.

^bData from *Evans et al.* [2004].

4.2.2. CO₂ Flux Calculations

4.2.2.1. Direct Dissolved Fluxes

[25] The CO₂ flux calculation includes both the direct flux of DIC measured in spring fluids and the degassing flux estimated from the δ¹³C_{DIC} data. Here we use the term “flux” to denote integrated mass transfer. The direct flux is calculated by multiplying the discharge [*Evans et al.*, 2004] (Table 4) for each spring by the total DIC concentrations. For the observed spring pHs and fluid chemistries [HCO₃⁻] ≅ alkalinity ≅ [DIC], but to account for the contribution of other carbonate species, we calculate the contribution of DIC from all species (ΣCO₂) using the following:

$$\Sigma\text{CO}_2 \cong [\text{HCO}_3^-] \cdot \left(1 + \frac{a_{\text{H}^+} \cdot \gamma_{\text{HCO}_3^-}}{K_1} + \frac{K_2 \cdot \gamma_{\text{HCO}_3^-}}{a_{\text{H}^+} \cdot \gamma_{\text{CO}_3^{2-}}} \right) \quad (7)$$

where [HCO₃⁻] is the bicarbonate concentration, a_{H⁺} is the activity of hydrogen ion, and K₁ and K₂ are the ionization constants for carbonic acid. The activity coefficients (γ_{*i*}) for bicarbonate and carbonate ion are calculated from an extended Debye-Huckel relationship [e.g., *Stumm and Morgan*, 1996]. In most cases ionic strengths are <0.2, and the Debye-Huckel calculation is sufficiently accurate for our purposes. The values for K₁ and K₂ and the activity coefficients are calculated for each spring system using the observed fluid exit-temperatures and standard carbonate equilibrium parameterizations [*Morse and Mackenzie*, 1990]. Results are summarized in Table 4.

4.2.2.2. Degassed Fluxes

[26] To produce the δ¹³C_{DIC} measured in the hot springs requires substantial CO₂ loss, with the

exact amount depending strongly on the initial δ¹³C_{DIC} of the fluid and the temperature interval over which degassing occurs, as well as the details of the degassing mechanism. The model calculation of isotopic fractionation during decarbonation of LH carbonates, the fluid inclusion data, and the gas composition from the Lo Mantang site are all consistent with an upper bound of δ¹³C_{DIC} in the undegassed fluid near +2‰. Degassing of this fluid below 125° C will drive off isotopically “light” CO₂, leaving the remaining DIC with δ¹³C > +2‰ (Figure 6). We therefore calculate the fraction of DIC lost to degassing (F_{exit T}) for each of the four spring systems with δ¹³C_{DIC} > +2‰ (Table 4) using our Rayleigh degassing model and assuming that degassing is primarily accompanied by carbonate precipitation (equations (2)–(4)). We estimate mean spring system δ¹³C_{DIC} and DIC values from the most active springs in each basin, using samples from the 2001 field season to ensure consistency in sample handling. For the four most ¹³C-enriched systems we calculate the amount of degassing necessary to produce δ¹³C_{DIC} values of +5.4‰, +11.0‰, +3.3‰, +6.0‰, as observed for the Seti Khola, Marsyandi, Bhuri Gandaki, and Trisuli systems, respectively, at their measured exit temperatures (Tables 1 and 4). We do not include the Lo Mantang system in the flux calculation as we lack data on discharge. The calculated CO₂ flux from each spring system is shown in Table 4. The calculation is sensitive both to the initial δ¹³C_{DIC} and to T. We use the maximum expected initial δ¹³C from decarbonation of LH metasediments (+2‰), which as noted is consistent with the maximum observed fluid inclusion values; using a lower value more typical of the average fluid inclusion data would increase the degassed fraction and thus the total CO₂ flux. We use the observed

surface fluid temperatures (40–70°C), but it is almost certain that degassing begins at higher temperatures in the sub-surface. The fractionation factor for $\text{CO}_2(\text{g})\text{—HCO}_3^-$ decreases with increasing T, and so a higher mean temperature of degassing would require greater $\text{CO}_2(\text{g})$ loss to produce the observed $\delta^{13}\text{C}_{\text{DIC}}$ values. With our conservative assumptions we obtain fractional degassing values (fraction of CO_2 lost) of 69%, 97%, 39%, and 79% for the Seti, Marsyandi, Bhuri, and Trisuli systems, respectively (Table 4). As noted above, the degassing fraction for the Lo Mantang system is $\geq 95\%$, although we do not use this in the flux calculation. For the Myagdi, Kali, and Modi systems with $\delta^{13}\text{C}_{\text{DIC}}$ near -7% , -9% , and $+2\%$, respectively, we did not make any degassing calculation, although they are supersaturated with CO_2 . We cannot reliably constrain the initial fluid compositions for these springs. They must be ^{13}C -depleted, but given the wide range of possible initial fluid $\delta^{13}\text{C}$ values indicated by the fluid inclusion data, and the sensitivity of the Rayleigh calculation to this value, we cannot estimate the fractional degassing without large uncertainty. Consequently, the total CO_2 flux that we obtain is an underestimate, since our assumptions are designed to minimize it.

[27] Recent independent work demonstrates that there is substantial diffuse CO_2 degassing near the hot springs at Syrabu Bensi, along the Trisuli River with magnitudes similar to the largest known sources in volcanic areas [Perrier *et al.*, 2008]. The authors use direct measurement with accumulation chambers to show that the degassed CO_2 flux from the area surrounding the spring-head is $\sim 6.3 \text{ mol a}^{-1}$, about 40–50X the alkalinity for the spring (1.5 mol a^{-1}). This would imply that ca. 98% of the dissolved CO_2 had degassed, a result somewhat higher than we obtain but still consistent with our findings. For the Trisuli, we estimate that a minimum of 79% degassing has occurred (Table 4).

4.2.2.3. Consumption by Weathering

[28] The alkalinity flux in the Narayani river system is primarily derived from the weathering of carbonate rocks, with only about 10% derived from the alteration of silicates [Evans *et al.*, 2004]. We have previously used Ge/Si and major ion data to estimate the fraction of silicate-derived alkalinity in the Narayani watershed contributed by hot springs at $\geq 10\%$, although the springs contribute $< 1\%$ of the total river discharge [Evans *et al.*, 2004]. Following France-Lanord and Derry [1997], long-term CO_2 consumption in the Narayani basin

is calculated from the annual river flux estimates of silicate derived cations as: $-\Delta\text{CO}_2 = (0.15 \times \text{Na}^{**})_{\text{sil}} + (0.10 \times \text{K}^*)_{\text{sil}} + (\text{Ca})_{\text{sil}} + (\text{Mg})_{\text{sil}} = 3.4 \times 10^9 \text{ mol CO}_2 \text{ a}^{-1}$ where Na^{**} and K^* are the fluxes of sodium and potassium corrected for cyclic salts/atmospheric deposition. The data on silicate-derived cation fluxes in the Narayani river are from Evans *et al.* [2004, Tables 4b and 7].

4.2.3. Total CO_2 Flux

[29] On a river-by-river basis, we combine the estimate of geothermal DIC flux to the rivers with degassing calculations based on the observed exit temperatures and $\delta^{13}\text{C}_{\text{DIC}}$ values of the sampled hot spring fluids to estimate the total metamorphic CO_2 flux to the surface environment in the Narayani basin (Table 4). The direct flux of hot spring DIC to the river system is $1.4 \times 10^9 \text{ mol a}^{-1}$ (Table 4) or about 42% of the weathering consumption of CO_2 by silicate weathering in the Narayani basin, $3.4 \times 10^9 \text{ mol a}^{-1}$ [France-Lanord *et al.*, 2003; Evans *et al.*, 2004]. Inclusion of the degassing flux raises the total CO_2 release by geothermal systems to $1.4 \times 10^{10} \text{ mol a}^{-1}$, about 4 times larger than the weathering uptake. Thus the net carbon balance from metamorphic devolatilization and transport to the surface in geothermal systems (which releases CO_2) and weathering (which consumes it) in the hydrologic system of a large area of the central Nepal Himalaya is almost certainly positive, and total CO_2 release exceeds weathering uptake.

[30] Our estimate of the degassing flux is based only on those springs with $\delta^{13}\text{C}_{\text{DIC}} > 2\%$, assumes no degassing takes place above the observed fluid exit temperatures, and takes the maximum observed crustal fluid value from the fluid inclusion data as the initial condition. Each of these choices minimizes the calculated degassing flux from the high $\delta^{13}\text{C}_{\text{DIC}}$ springs. We have focused on modeling degassing in springs with high $\delta^{13}\text{C}_{\text{DIC}}$ because we can establish a maximum $\delta^{13}\text{C}$ for the initial fluid compositions from our fluid inclusion data. Consequently, our degassing calculation includes only selected geothermal systems from the Seti, Marsyandi, Bhuri, and Trisuli subbasins which span a $\sim 100\text{km}$ swath of the central Nepal Himalaya (Figure 1). Other spring systems within the Narayani are supersaturated with CO_2 and almost certainly are partially degassed but have negative to near-zero $\delta^{13}\text{C}_{\text{DIC}}$ values, such as the Myagdi ($\delta^{13}\text{C}_{\text{DIC}} = -7\%$). Low $\delta^{13}\text{C}_{\text{DIC}}$ in Himalayan springs with abundant DIC can arise if CO_2 is ultimately derived from sedimentary organic carbon, either through oxidation or isotopic exchange

between CO_2 and CH_4 at temperatures $>250^\circ\text{C}$ [Giggenbach, 1997]. Since we cannot reliably constrain the initial value of the low $\delta^{13}\text{C}_{\text{DIC}}$ fluids we cannot make reliable estimates of the degree of fractionation and degassing for these springs, and therefore only include the direct DIC flux from those systems, which is a strong lower limit of the total CO_2 flux from these low $\delta^{13}\text{C}_{\text{DIC}}$ springs. We also make no attempt to constrain the contribution of the diffuse degassing (nongeothermal) flux, which can be considerable [Perrier *et al.*, 2008]. Our assumptions clearly lead to an underestimate of the total CO_2 degassing flux, and our result that the net CO_2 flux from central Nepal is significantly positive appears robust, even given uncertainties in the degassing model. For example, if we were to ignore degassing altogether, we still find that the direct geothermal DIC flux is $> 40\%$ of the weathering uptake. The occurrence of even modest degassing therefore implies that the overall geothermal flux is at least as large as the weathering flux. Better constraints on near-surface degassing processes will help refine estimates of the carbon balance in this system.

5. Conclusions

[31] Hot springs are found along the entire Himalayan front [Oldham, 1883; Barnes *et al.*, 1978; Bhattarai, 1980; Shankar *et al.*, 1991]. The Narayani basin comprises 150 km of the total Himalayan arc length of 2500 km, or 6%. If the geothermal degassing and DIC flux from the Narayani basin can be extrapolated as a first approximation of the CO_2 flux to the surface from Himalayan metamorphism, about $2 \times 10^{11} \text{ mol a}^{-1}$ of CO_2 is released along the Himalayan arc. Such a flux is 7 to 60% of recent estimates of the global flux from volcanic arcs, in the range $0.35\text{--}3.1 \times 10^{12} \text{ mol a}^{-1}$ [Marty and Tolstikhin, 1998; Gorman and Kerrick, 2006]. While such an extrapolation is simple, only additional data from along strike in the Himalayan arc can establish whether it is realistic and how strong a CO_2 source the Himalayan collision zone is.

[32] In the Himalaya, CO_2 consumption is ultimately limited by a strongly weathering-limited regime which leads to low weathering intensity, and rock types that are low in Ca and Mg silicates and so are inefficient sinks for CO_2 [France-Lanord and Derry, 1997]. Metamorphism of carbonate-pelite sediments associated with the ongoing India-Asia collision provides a quantitatively important source of CO_2 to the surface environment. Our

data provide the first data-driven large-scale estimate of the metamorphic degassing flux from an active collisional orogen utilizing samples from the 32,000-km² Narayani basin. We find that Himalayan metamorphic processes provide a source of CO_2 that is larger than the consumption of CO_2 by weathering of Himalayan rocks. Our data imply that the net CO_2 flux to the ocean-atmosphere system from Himalayan orogenesis is positive, not strongly negative as has been widely assumed. Contrary to conventional wisdom continental collision events should not necessarily result in CO_2 drawdown via perturbation of the carbonate-silicate geochemical cycle. A persistent difficulty in geological carbon cycle models is the exact nature of the feedback between changes in atmospheric CO_2 levels and weathering rates necessary to stabilize the models on long timescales. If collisional orogenic events produce and consume CO_2 at roughly the same rate the need for a strong, climate-driven feedback to compensate for orogenic perturbations to the carbon cycle may be relaxed.

Notation

Na^*	$[\text{Na}^+] - [\text{Cl}^-]$
Na^{**}	$[\text{Na}^+] - [\text{Cl}^-] - [\text{Na}^+] \text{ from atmospheric deposition}$
K^*	$[\text{K}^+] - [\text{K}^+] \text{ from atmospheric deposition}$
Q_{HS}	Hot spring discharge
$\delta^{13}\text{C}_{\text{DIC}}$	$\delta^{13}\text{C}$ value for dissolved inorganic carbon in hot spring waters
$\delta^{13}\text{C}_{\text{CO}_2}$	$\delta^{13}\text{C}$ value for carbon dioxide gas
$\delta_{\text{HCO}_3^-}$	$\delta^{13}\text{C}$ value for bicarbonate ion
$\delta_{\text{CO}_2}^{\text{instant}}$	$\delta^{13}\text{C}$ value for instantaneous production of $\text{CO}_2(\text{g})$
$\delta_{\text{CO}_2}^{\text{cum}}$	$\delta^{13}\text{C}$ value for cumulative production of $\text{CO}_2(\text{g})$
$\alpha_{\text{HCO}_3^- - \text{CO}_2}$	equilibrium isotope fractionation factor for $\text{HCO}_3^- - \text{CO}_2(\text{g})$
$\alpha_{\text{CaCO}_3 - \text{CO}_2}$	equilibrium isotope fractionation factor for $\text{CaCO}_3 - \text{CO}_2(\text{g})$
a_{H^+}	activity of hydrogen ion
K_1	ionization constant for carbonic acid
K_2	ionization constant for bicarbonate
(γ_i)	activity coefficients for bicarbonate and carbonate ion
R_{DIC}^0	$^{13}\text{C}/^{12}\text{C}$ of the DIC in the initial crustal fluid prior to degassing

- R_{DIC} $^{13}\text{C}/^{12}\text{C}$ of DIC in spring fluids
 after degassing
 α temperature dependent fractionation
 between HCO_3^- (aq) and CO_2 (g)
 f the fraction of dissolved CO_2
 remaining after degassing

Acknowledgments

[33] The authors wish to thank Patrick Le Fort who initiated part of this research. This work was funded in part by NSF grant EAR0087671 and by the CNRS. We also thank D. Newell and an anonymous reviewer for their helpful reviews.

References

- Amundson, R., and E. Kelly (1987), The chemistry and mineralogy of a CO_2 -rich travertine depositing spring in the California Coast Range, *Geochim. Cosmochim. Acta*, *51*(11), 2883–2890.
- Avouac, J. P., and E. B. Burov (1996), Erosion as a driving mechanism of intracontinental mountain growth, *J. Geophys. Res.*, *101*(B8), 17,747–17,769.
- Barnes, I., et al. (1978), Global distribution of carbon dioxide discharges and major zones of seismicity, *U.S. Geol. Surv. Map*, 1-1528, 10 pp.
- Berner, R. A., et al. (1983), The carbonate-silicate geochemical cycle and its effect on atmospheric carbon dioxide over the past 100 million years, *Am. J. Sci.*, 641–683.
- Bhattarai, D. R. (1980), Some geothermal springs of Nepal, *Tectonophysics*, *62*, 7–11.
- Bickle, M. J. (1996), Metamorphic decarbonation, silicate weathering and the long-term carbon cycle, *Terra Nova*, *8*, 270–276.
- Bogacz, W., and M. Kotarba (1981), Structural mesoscopic studies in the Kali Gandaki thermal springs area (Nepal Himalayas), *Bull. Polish Acad. of Sci. Earth Sci.*, *29*, 293–301.
- Boullier, A. M., et al. (1991), Linked fluid and tectonic evolution in the High Himalaya mountains (Nepal), *Contrib. Mineral. Petrol.*, *107*, 358–372.
- Bollinger, L., et al. (2006), Mountain building in the Nepal Himalaya: Thermal and kinematic model, *Earth Planet. Sci. Lett.*, *244*(1–2), 58–71.
- Chacko, T., et al. (1991), Oxygen and carbon isotope fractionations between CO_2 and calcite, *Geochim. Cosmochim. Acta*, *55*(10), 2867–2882.
- Chafetz, H. S., et al. (1991), Microenvironmental controls on mineralogy and habit of CaCO_3 precipitates - An example from an active travertine system, *Sedimentology*, *38*(1), 107–126.
- Chamberlain, C. P., et al. (2002), Overview of hydrothermal activity associated with active orogenesis and metamorphism: Nanga Parbat, Pakistan Himalaya, *Am. J. Sci.*, *302*(8), 726–748.
- Clayton, R. N., et al. (1972), Oxygen isotope fractionation between quartz and water, *J. Geophys. Res.*, *77*, 3057–3067.
- Clift, P. D. (2006), Controls on the erosion of Cenozoic Asia and the flux of clastic sediment to the ocean, *Earth Planet. Sci. Lett.*, *241*(3–4), 571–580.
- Colchen, M., et al. (1986), Notice explicative de la carte géologique Annapurna-Manaslu-Ganesh (Himalaya du Népal) au 1:200.000e (bilingue: français-anglais), Cent. Natl. de la Rech. Sci., Paris.
- Craw, D. (1990), Fluid evolution during uplift of the Annapurna Himal, central Nepal., *Lithos*, *24*, 137–150.
- Curry, J. R. (1994), Sediment volume and mass beneath the Bay of Bengal, *Earth Planet. Sci. Lett.*, *125*, 371–383.
- Dandurand, J. L., et al. (1982), Kinetically controlled variations of major components and carbon and oxygen isotopes in a calcite-precipitating spring, *Chem. Geol.*, *36*(3–4), 299–315.
- Darling, R. S., et al. (2003), Refining the Himalayan retrograde metamorphic path: Evidence from fluid inclusions in undeformed quartz veins, central Nepal, *Geol. Soc. of Am. Abstr. Progr.*, *35*(6), 327.
- Derry, L. A., and M. J. Evans (2002), Geochemical constraints on geothermal heat flow in the central Nepal Himalaya, *Eos Trans. AGU*, *83*(47), Fall Meet. Suppl., Abstract T71A-1163.
- Dulinski, M., et al. (1995), Stable-isotope composition of spelean calcites and gaseous CO_2 from Tylicz (Polish Carpathians), *Chem. Geol.*, *125*(3–4), 271–280.
- Evans, M. J. (2002), Geothermal fluxes of solutes, heat, and carbon to central Nepal rivers, 225 pp, Cornell University, Ithaca, N.Y.
- Evans, M. J., et al. (2004), Geothermal fluxes of alkalinity in the Narayani river system of central Nepal, *Geochem. Geophys. Geosyst.*, *5*, Q08011, doi:10.1029/2004GC000719.
- France-Lanord, C. (1987), Chevauchement, métamorphisme et magmatisme en Himalaya du Népal central. Etude isotopique H, C, O., 246 pp, Inst. Natl. Polytech. de Lorraine, Nancy, France.
- France-Lanord, C., and L. A. Derry (1997), Organic carbon burial forcing of the carbon cycle from Himalayan erosion, *Nature*, *390*(6655), 65–67.
- France-Lanord, C., et al. (2003), Annual dissolved fluxes from Central Nepal rivers: Budget of chemical erosion in the Himalayas, *Comptes Rendu Geosci.*, *335*(16), 1131–1140.
- Friedman, I. (1970), Some investigations of the deposition of travertine from Hot Springs-I. The isotopic chemistry of a travertine-depositing spring, *Geochim. Cosmochim. Acta*, *34*, 1303–1315.
- Gaillardet, J., et al. (1999), Global silicate weathering and CO_2 consumption rates deduced from the chemistry of large rivers, *Chem. Geol.*, *159*(1–4), 3–30.
- Gajurel, A., et al. (2006), C and O isotope compositions of modern fresh-water mollusc shells and river waters from Himalaya and Ganga plain, *Chem. Geol.*, *233*(1–2), 156–183.
- Galy, A., and C. France-Lanord (1999), Weathering processes in the Ganges-Brahmaputra basin and the riverine alkalinity budget, *Chem. Geol.*, *159*(1–4), 31–60.
- Gardner, R., and N. Walsh (1996), Chemical weathering of metamorphic rocks from low elevations in the southern Himalaya, *Chem. Geol.*, *127*(1–3), 161–176.
- Garzanti, E., et al. (2007), Quantifying sand provenance and erosion (Marsyandi River Nepal Himalaya), *Earth Planet. Sci. Lett.*, *258*(3–4), 500–515.
- Garzzone, C. N., et al. (2000), Predicting paleoelevation of Tibet and the Himalaya from delta O-18 vs. altitude gradients in meteoric water across the Nepal Himalaya, *Earth Planet. Sci. Lett.*, *183*(1–2), 215–229.
- Giggenbach, W. F. (1997), Relative importance of thermodynamic and kinetic processes in governing the chemical and isotopic composition of carbon gases in high-heatflow sedimentary basins, *Geochim. Cosmochim. Acta*, *61*(17), 3763–3785.
- Goodbred, S. L., and S. A. Kuehl (2000), Enormous Ganges-Brahmaputra sediment discharge during strengthened early Holocene monsoon, *Geology*, *28*(12), 1083–1086.

- Gorman, P. J., and D. M. Kerrick (2006), Modeling open system metamorphic decarbonation of subducting slabs, *Geochem. Geophys. Geosyst.*, 7, Q04007, doi:10.1029/2005GC001125.
- Grabczak, J., and M. Kotarba (1985), Isotopic composition of the thermal waters in the central part of the Nepal Himalayas, *Geothermics*, 14, 567–576.
- Guo, L., et al. (1996), Possible microbial effects on stable carbon isotopes in hot-spring travertines, *J. Sediment. Res.*, 66(3), 468–473.
- Hodges, K. V., et al. (2004), Quaternary deformation, river steepening, and heavy precipitation at the front of the Higher Himalayan ranges, *Earth Planet. Sci. Lett.*, 220(3–4), 379–389.
- Jenkin, G. R. T., et al. (1994), Stable isotopic and fluid inclusion evidence for meteoric fluid penetration into an active mountain belt-Alpine schist, New Zealand, *J. Meteorol. Geol.*, 12(4), 429–444.
- Kerrick, D. M. (2001), Present and past nonanthropogenic CO₂ degassing from the solid Earth, *Rev. Geophys.*, 39(4), 565–585.
- Kerrick, D. M., and K. Caldeira (1998), Metamorphic CO₂ degassing from orogenic belts, *Chem. Geol.*, 145(3–4), 213–232.
- Koons, P. O., and D. Craw (1991), Evolution of fluid driving forces and composition within collisional orogens., *Geophys. Res. Lett.*, 18(5), 935–938.
- Kotarba, M., et al. (1981), Hydrogeological investigations in the Kali Gandaki thermal springs area (Nepal Himalayas), *Bull. Polish Acad. Sci. Earth Sci.*, 29, 283–291.
- Lave, J., and J. P. Avouac (2001), Fluvial incision and tectonic uplift across the Himalayas of central Nepal, *J. Geophys. Res.*, 106(B11), 26,561–26,591.
- Lemonnier, C., et al. (1999), Electrical structure of the Himalaya of Central Nepal: high conductivity around the mid-crustal ramp along the MHT, *Geophys. Res. Lett.*, 26(21), 3261–3264.
- Marty, B., and I. N. Tolstikhin (1998), CO₂ fluxes from mid-ocean ridges, arcs and plumes, *Chem. Geol.*, 145, 233–248.
- Marty, B., et al. (1996), CO₂ and Helium in mineral springs of Nepal and Mustang: A study of volatile release processes during the Himalayan Tectonics, paper presented at 11th Himalaya-Karakorum-Tibet Workshop, Flagstaff, Ariz.
- Michaelis, J., et al. (1985), Partitioning of ¹³C and ¹²C on the Degassing of CO₂ and the Precipitation of Calcite - Rayleigh-Type Fractionation and a Kinetic-Model, *Am. J. Sci.*, 285(4), 318–327.
- Millot, R., et al. (2002), The global control of silicate weathering rates and the coupling with physical erosion: new insights from rivers of the Canadian Shield, *Earth Planet. Sci. Lett.*, 196(1–2), 83–98.
- Mook, W. G., et al. (1974), Carbon isotope fractionation between dissolved bicarbonate and gaseous carbon dioxide, *Earth Planet. Sci. Lett.*, 22(2), 169–176.
- Morse, J. W., and F. T. Mackenzie (1990), *Geochemistry of Sedimentary Carbonates*, 707 pp., Elsevier Sci., New York.
- Oldham, T. (1883), The thermal springs of India, *Mem. Geol. Surv. India*, 19, 99–140.
- Pandey, M. R., et al. (1995), Interseismic strain accumulation on the Himlayan crustal ramp (Nepal), *Geophys. Res. Lett.*, 22, 751–754.
- Pêcher, A. (1979), Les inclusions fluides des quartz d'exsudation de la zone du M. C.T. himalayen au Népal central: données sur la phase fluide dans une grande zone de cisaillement crustal., *Bull. Minéral.*, 102, 537–554.
- Pentecost, A. (1995), Geochemistry of carbon dioxide in six travertine-depositing waters of Italy, *J. Hydrol.*, 167(1–4), 263–278.
- Perrier, F., et al. (2008), High carbon dioxide and radon-222 gas exhalation at the Syabru-Bensi hot springs in Central Nepal, *Earth Planet. Sci. Lett.*, in press.
- Raymo, M. E., and W. F. Ruddiman (1992), Tectonic forcing of late Cenozoic climate, *Nature*, 359, 117–122.
- Riebe, C. S., et al. (2001), Strong tectonic and weak climatic control of long-term chemical weathering rates, *Geology*, 29(6), 511–514.
- Romanek, C. S., et al. (1992), Carbon isotopic fractionation in synthetic aragonite and calcite - Effects of temperature and precipitation rate, *Geochim. Cosmochim. Acta*, 56(1), 419–430.
- Schelling, D., and K. Arita (1991), Thrust Tectonics, Crustal Shortening, and the Structure of the Far-Eastern Nepal Himalaya, *Tectonics*, 10(5), 851–862.
- Seeber, L., and V. Gornitz (1983), River profiles along the Himalayan Arc as indicators of active tectonics, *Tectonophysics*, 92(4), 335–367.
- Silverstone, J., and D. S. Gutzler (1993), Post-125 Ma carbon storage associated with continent-continent collision, *Geology*, 21, 885–888.
- Shankar, R., et al. (1991), *Geothermal Atlas of India*, 144 pp., Geol. Surv. of India, Kolkata.
- Shipton, Z. K., et al. (2004), Analysis of CO₂ leakage through “low-permeability” faults from natural reservoirs in the Colorado Plateau, southern Utah, in *Geological Storage of Carbon Dioxide*, edited by S. J. Baines and R. H. Worden, pp. 43–58, Geol. Soc. of London.
- Singh, R., et al. (2004), Geochemistry of thermal springs from Bhutan Himalaya, *J. Geol. Soc. India*, 64(2), 191–198.
- Stumm, W., and J. J. Morgan (1996), *Aquatic Chemistry*, 1042 pp., John Wiley, New York.
- Szaran, J. (1997), Achievement of carbon isotope equilibrium in the system HCO₃⁻ (solution) CO₂ (gas), *Chem. Geol.*, 142(1–2), 79–86.
- Templeton, A. S., et al. (1998), Stable isotopic evidence for mixing between metamorphic fluids and surface-derived waters during recent uplift of the Southern Alps, New Zealand, *Earth Planet. Sci. Lett.*, 154(1–4), 73–92.
- Walker, J. C. G., et al. (1981), A negative feedback mechanism for the long-term stabilization of the Earth's surface temperature, *J. Geophys. Res.*, 86, 9776–9782.
- West, A. J., et al. (2002), Small-catchment perspective on Himalayan weathering fluxes, *Geology*, 30(4), 355–358.
- Whipp, D. M., and T. A. Ehlers (2007), Influence of groundwater flow on thermochronometer-derived exhumation rates in the central Nepalese Himalaya, *Geology*, 35(9), 851–854.
- Whipp, D. M., et al. (2007), Plio-Quaternary exhumation history of the central Nepalese Himalaya: 2. Thermokinematic and thermochronometer age prediction model, *Tectonics*, 26, TC3003, doi:10.1029/2006TC001991.
- Wobus, C., et al. (2005), Active out-of-sequence thrust faulting in the central Nepalese Himalaya, *Nature*, 434(7036), 1008–1011.
- Wobus, C. W., et al. (2003), Has focused denudation sustained active thrusting at the Himalayan topographic front?, *Geology*, 31(10), 861–864.